This is a repository copy of *Finite element simulations of hyperpolarized gas DWI in micro-CT meshes of acinar airways: validating the cylinder and stretched exponential models of lung microstructural length scales*.

White Rose Research Online URL for this paper:
https://eprints.whiterose.ac.uk/171703/

Version: Published Version

Article:

Chan, H.-F. orcid.org/0000-0002-5382-2097, Collier, G. orcid.org/0000-0002-1874-4775, Parra-Robles, J. et al. (1 more author) (2021) Finite element simulations of hyperpolarized gas DWI in micro-CT meshes of acinar airways: validating the cylinder and stretched exponential models of lung microstructural length scales. Magnetic Resonance in Medicine, 86 (1). pp. 514-525. ISSN 0740-3194

https://doi.org/10.1002/mrm.28703

Reuse
This article is distributed under the terms of the Creative Commons Attribution (CC BY) licence. This licence allows you to distribute, remix, tweak, and build upon the work, even commercially, as long as you credit the authors for the original work. More information and the full terms of the licence here:
https://creativecommons.org/licenses/

Takedown
If you consider content in White Rose Research Online to be in breach of UK law, please notify us by emailing eprints@whiterose.ac.uk including the URL of the record and the reason for the withdrawal request.

eprints@whiterose.ac.uk
https://eprints.whiterose.ac.uk/

Received: 17 June 2020 | Revised: 7 December 2020 | Accepted: 7 January 2021

DOI: 10.1002/mrm.28703

FULL PAPER

Magnetic Resonance in Medicine

Finite element simulations of hyperpolarized gas DWI in micro-CT meshes of acinar airways: validating the cylinder and stretched exponential models of lung microstructural length scales

Ho-Fung Chan[1] | **Guilhem J. Collier**[1] | **Juan Parra-Robles**[1,2] | **Jim M. Wild**[1,3]

[1]POLARIS, Department of Infection, Immunity & Cardiovascular Disease, University of Sheffield, Sheffield, United Kingdom

[2]Faculty of Pharmacy, Universidad Complutense de Madrid, Madrid, Spain

[3]Insigneo, Institute for in Silico Medicine, University of Sheffield, Sheffield, United Kingdom

Correspondence
Jim M. Wild, POLARIS, Department of Infection, Immunity & Cardiovascular Disease, University of Sheffield, C Floor, Royal Hallamshire Hospital, Glossop Road, Sheffield, S10 2JF, UK.
Email: j.m.wild@sheffield.ac.uk

Funding information
Supported by National Institute for Health Research (NIHR) grant NIHR-RP-R3-12-027 and Medical Research Council (MRC) grant MR/M008894/1

Purpose: This work assesses the accuracy of the stretched exponential (SEM) and cylinder models of lung microstructural length scales that can be derived from hyperpolarized gas DWI. This was achieved by simulating ^{3}He and ^{129}Xe DWI signals within two micro-CT–derived realistic acinar airspace meshes that represent healthy and idiopathic pulmonary fibrosis lungs.

Methods: The healthy and idiopathic pulmonary fibrosis acinar airway meshes were derived from segmentations of 3D micro-CT images of excised human lungs and meshed for finite element simulations of the Bloch-Torrey equations. ^{3}He and ^{129}Xe multiple *b* value DWI experiments across a range of diffusion times (^{3}He $\Delta = 1.6$ ms; ^{129}Xe $\Delta = 5$ to 20 ms) were simulated in each mesh. Global SEM mean diffusive length scale and cylinder model mean chord length value was derived from each finite element simulation and compared against each mesh's mean linear intercept length, calculated from intercept length measurements within micro-CT segmentation masks.

Results: The SEM-derived mean diffusive length scale was within ±10% of the mean linear intercept length for simulations with both ^{3}He ($\Delta = 1.6$ ms) and ^{129}Xe ($\Delta = 7$ to 13 ms) in the healthy mesh, and with ^{129}Xe ($\Delta = 13$ to 20 ms) for the idiopathic pulmonary fibrosis mesh, whereas for the cylinder model–derived mean chord length the closest agreement with mean linear intercept length (11.7% and 22.6% difference) was at ^{129}Xe $\Delta = 20$ ms for both healthy and IPF meshes, respectively.

Conclusion: This work validates the use of the SEM for accurate estimation of acinar dimensions and indicates that the SEM is relatively robust across a range of experimental conditions and acinar length scales.

KEYWORDS

cylinder airway model, finite element simulations, hyperpolarized gas DWI, lung morphometry, micro-CT, stretched exponential model

This is an open access article under the terms of the Creative Commons Attribution License, which permits use, distribution and reproduction in any medium, provided the original work is properly cited.

© 2021 The Authors. *Magnetic Resonance in Medicine* published by Wiley Periodicals LLC on behalf of International Society for Magnetic Resonance in Medicine.

1 | INTRODUCTION

The detection of microstructural changes to the acinar airways, the structural units of gas exchange of the lungs that are located distally to the terminal bronchioles, are crucial for the clinical evaluation and longitudinal monitoring of a range of pulmonary diseases. Multi-detector CT is the current clinical gold standard for in vivo structural evaluation of the lungs in emphysema[1-3] and interstitial lung diseases.[4,5] However, multi-detector CT cannot resolve airways smaller than approximately 1.5 mm in diameter,[6] corresponding to the seventh to ninth generation of airways.[7] The higher spatial resolution of micro-CT facilitates 3D visualization of the acinar airways in ex vivo human lung samples and has been used to investigate chronic obstructive pulmonary disease mechanisms in the small airways and terminal bronchioles that previously could not be resolved with in vivo multi-detector CT.[8,9]

DWI with inhaled hyperpolarized gases (^{3}He or ^{129}Xe) combines the advantages of both multi-detector CT and micro-CT with 3D in vivo information of the lung microstructure due to the Brownian gas atom diffusion restriction within the acinar airways. The derived ADC is a sensitive biomarker of underlying changes in acinar airway microstructure.[10,11] The cylinder airway model (CM)[12-14] and stretched exponential model (SEM)[15,16] are theoretical models of hyperpolarized gas DWI signal within the lungs that can derive estimates of in vivo acinar airway dimensions with both ^{3}He and ^{129}Xe gases. These two diffusion models have been used to elucidate quantitative changes in acinar airway microstructure that are additional to basic ADC or mean-square displacement $\left(\sqrt{2 \cdot \mathrm{ADC} \cdot t}\right)$ measurements associated with smoking-related early emphysema,[17] lung inflation mechanisms,[18] post-transplant lung growth[19] and lifespan,[20] aging,[21] and idiopathic pulmonary fibrosis (IPF) disease progression.[22]

The reproducibility and accuracy of derived morphometry measurements from hyperpolarized gas DWI models are crucial for their reliable use in the detection of therapeutic responses or longitudinal disease changes. Excellent short- and long-term reproducibility of diffusion model measurements have been demonstrated in healthy subjects,[23] whereas excellent same-day reproducibility has been shown in patients with IPF.[22]

To date, two validation methods have been used to assess the accuracy of measurements from the CM. The first method utilized direct validation of CM-derived morphological parameters obtained from ex vivo lung specimens against equivalent histological measurements in lung cores obtained from the same specimens.[13,24,25] Good agreement between CM and histology measurements was observed for morphological parameters of mean chord length (Lm) as well as outer acinar radius (R) and alveolar sleeve depth (h) in ex vivo human[13] and canine lungs,[24] respectively. A second proposed validation method was via computer simulations of hyperpolarized gas DWI within simplified geometrical models of acinar airways,[26-28] where known model dimensions were compared to respective CM-derived parameters obtained from Monte-Carlo or finite element (FE) simulations of ^{3}He gas diffusion. Simulations across a range of different diffusion parameters were used to establish an accurate operational range of the CM.

Recently, the SEM-derived mean diffusive length scale (Lm_D) was indirectly validated with comparisons against CM-derived measurements in the same subjects across a range of acinar length scales.[29] However, the Lm_D has not yet been directly validated against histology or known acinar geometries. Therefore, this work aims to validate the SEM Lm_D, alongside CM-derived parameters, with FE simulations of hyperpolarized ^{3}He and ^{129}Xe DWI in realistic models of acinar airway geometry–derived from micro-CT images. Specifically, FE simulations were used to determine optimum diffusion gradient parameters for accurate measurements with ^{3}He and ^{129}Xe and to establish the operational ranges of the SEM and CM by investigating the relationship between diffusion model measurements and experimental diffusion time.

2 | METHODS

2.1 | Acinar airway geometry meshes

Two different realistic acinar airspace geometry meshes were derived from existing 3D micro-CT images of human lung samples (16 μm resolution) representing healthy[8] and IPF[30] lungs (Figure 1). An IPF lung was chosen because IPF-related acinar airspace changes are subtle and not as well understood as emphysematous airspace enlargement, and because IPF may cause substantial deviation from the healthy alveolar duct cylindrical geometry.[7] The process used to obtain and prepare lung samples from explanted lungs for micro-CT are fully described in McDonough et al.[8] Written informed consent was obtained from the next of kin of the patients whose donated lungs served as healthy controls.[8] Written informed consent was obtained from all IPF patients, and the study was approved by the hospital ethics and university biosafety committees in Leuven, Belgium.[30] Digital micro-CT images for this work were obtained with principal investigator approval.

Segmentation of the 3D micro-CT images were performed in Simpleware ScanIP (v. 2016.09-SP1, Synopsys, Mountain View, CA) where de-noising and edge enhancement was used to first segment the alveolar walls, followed by inverting the alveolar wall mask to derive the acinar airspace.[31] A single connected region of acinar airspace (approximately the size of a single MRI voxel ~4 mm isotropic) was isolated by flood-filling the airspace mask after manual editing and Gaussian

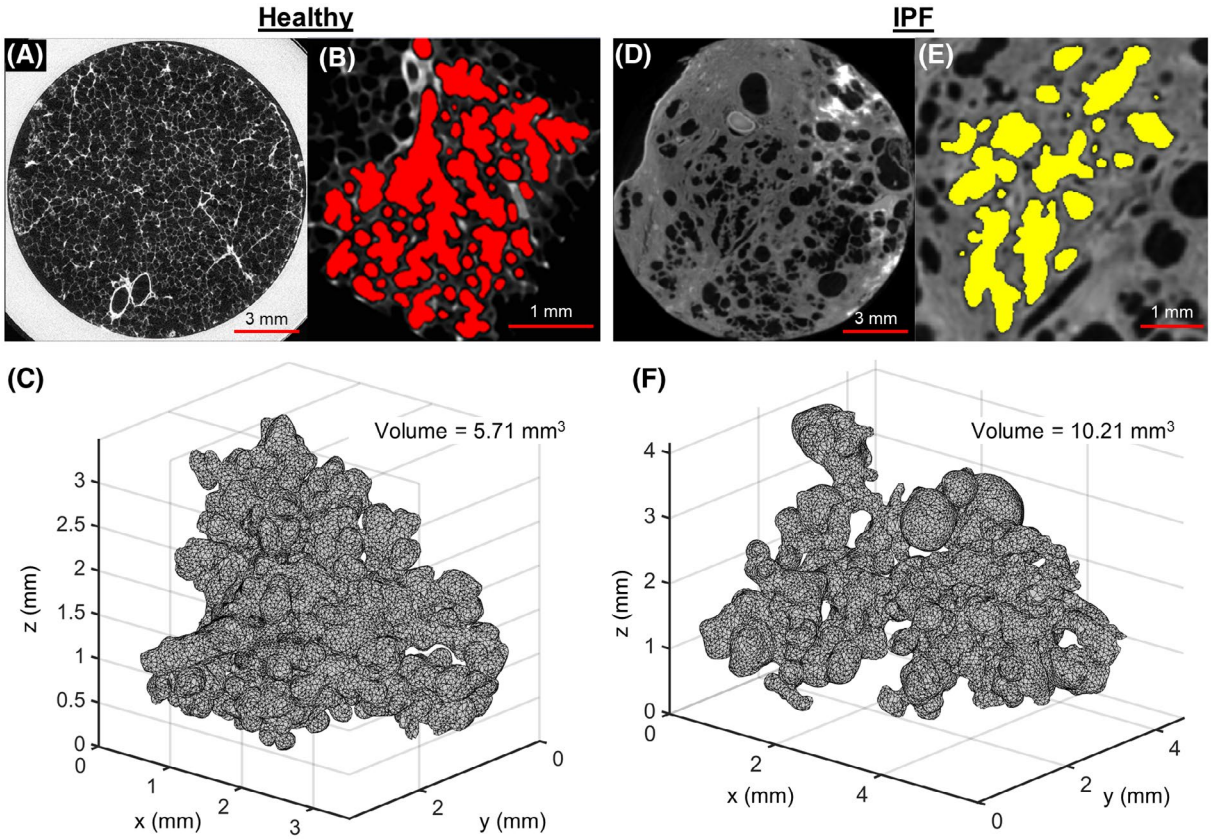

FIGURE 1 Representative healthy (A) and IPF (D) micro-CT images (16 μm resolution) obtained from human lung samples. Representative healthy (B) and IPF (E) acinar airspace masks after segmentation of a single connect region of acinar airspace using flood filling and manual editing. Tetrahedral FE meshes representative of healthy (C) and IPF (F) acinar airspace meshes. FE, finite element; IPF, idiopathic pulmonary fibrosis

smoothing. The resulting healthy and IPF acinar airspace geometries were then meshed for FE analysis with tetrahedral elements using the Simpleware FE Module (Synopsys). The final healthy and IPF acinar airspace FE meshes, after optimization (see Supporting Information), contained ~120,000 elements and ~37,000 nodes, and ~110,000 elements and ~36,000 nodes, respectively.

2.2 | Mean linear intercept length

The mean linear intercept length (MLI) for each micro-CT acinar airspace mesh was calculated as a benchmark for subsequent FE simulation–derived acinar airway dimensions from the two diffusion models. MLI is taken as being representative of the mean free path of restricted Brownian diffusion of the hyperpolarized gas atoms within the acinar airspace. MLI was calculated automatically from the segmented isolated acinar airspace micro-CT masks, which were up-sampled to an isotropic 4 μm resolution by direct measurements of linear intercept lengths in MATLAB (R2019a, MathWorks, Natick, MA) (Figure 2). Parallel grid lines spaced 80 μm apart were used to calculate intercept lengths across every mask image spaced 80 μm apart. This entire process is analogous to the stereologic method for chord length measurements used for estimating MLI[32,33] and was repeated for 31 different orientations in 3D space at 30° intervals, representing the different 1D diffusion-sensitizing gradient directions used in subsequent FE simulations. The MLI was obtained from the mean value of the distribution of all intercept lengths in all orientations. The MLI for the healthy and IPF acinar airway meshes were 266 μm and 371 μm, respectively, and are similar to histological MLI values reported for healthy and IPF human lung samples.[34,35] It is important to note that there is a small difference between the CM-derived *Lm* and histological MLI gas-space parameters. The derivation of CM *Lm* assumes a negligible alveolar wall or interstitium,[13] whereas in the calculation of MLI no assumptions about the interstitium are made.

2.3 | Finite element simulations

Hyperpolarized ^{3}He and ^{129}Xe multiple *b* value DWI experiments were simulated in the micro-CT acinar airspace meshes. The evolution of the MR signal from a Stejskal-Tanner pulsed

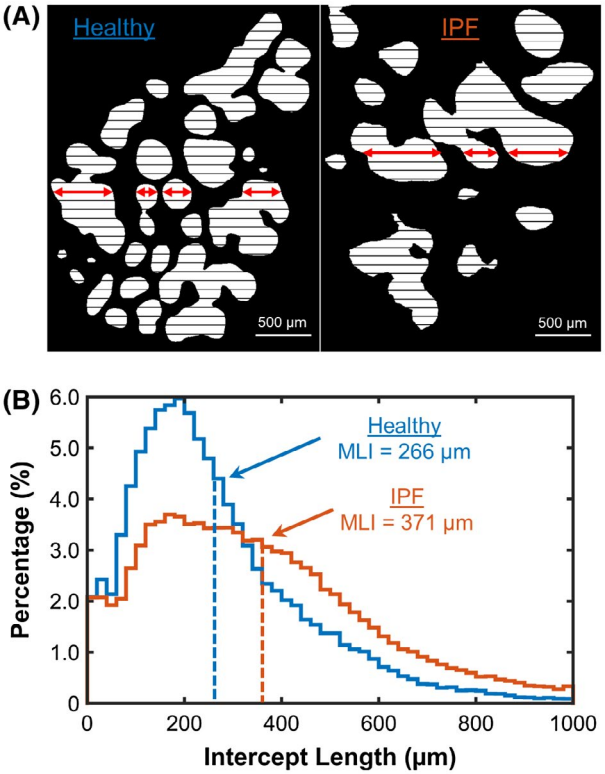

FIGURE 2 (A) Parallel grid lines, spaced 80 μm apart, across a representative healthy and IPF acinar airspace mask image where intercept lengths (red arrows) were calculated across each grid line. (B) Histograms of all intercept lengths across the entire healthy and IPF acinar airspace volume. The mean value of the distributions was the MLI. MLI, mean linear intercept length

gradient diffusion experiment,[36] proportional to the integral of transverse magnetization over a voxel, can be described by the Bloch-Torrey equation[37]:

$$\frac{\partial M(\vec{r},t)}{\partial t} = i\gamma\left[G(\vec{r},t)\cdot\vec{r}\right]M(\vec{r},t) + D_0\nabla^2 M(\vec{r},t), \quad (1)$$

where $M(\vec{r},t)$ is the spatially varying complex transverse magnetization; γ is the gyromagnetic ratio of ^{3}He or ^{129}Xe; $G(\vec{r},t)$ is a spatially varying magnetic field gradient; and D_0 is the ^{3}He or ^{129}Xe free diffusion coefficient. In hyperpolarized gas DWI experiments, $G(\vec{r},t)$ is typically a bipolar trapezoidal gradient waveform used to sensitize the MR signal to diffusion attenuation, and the b value (b) is given by[12]:

$$b = \gamma^2 G^2\left[\delta^2\left(\Delta - \frac{\delta}{3}\right) + \tau\left(\delta^2 - 2\Delta\delta + \Delta\tau - \frac{7}{6}\delta\tau + \frac{8}{15}\tau^2\right)\right], \quad (2)$$

where G is the gradient amplitude; Δ is the diffusion time; δ is the gradient lobe time; and τ is the ramp time. The diffusion time (Δ) is defined as the duration from the middle of the first gradient lobe to the middle of the second. A typical in vivo ^{3}He and ^{129}Xe DWI voxel contains numerous acinar airways of various orientations that all contribute to the measured DWI signal. Therefore, to simulate in vivo conditions, diffusion FE simulations were implemented in a single direction and solved for 31 different 1D diffusion-sensitizing gradient angles uniformly orientated in 3D space at 30° intervals.[28]

A range of validation experiments were performed in the two acinar airspace meshes with both ^{3}He and ^{129}Xe gases at different diffusion times to explore the full operational range of the two theoretical hyperpolarized gas diffusion models. For each FE simulation, the same following diffusion parameters were simulated, unless otherwise stated, for either ^{3}He: $D_0 = 0.88$ cm^2/s and b = [0, 1.6, 3.2, 4.8, 6.4, 8.0] s/cm^2 or for ^{129}Xe: $D_0 = 0.14$ cm^2/s and b = [0, 6, 12, 18, 24, 30] s/cm^2. The choice of D_0 reflects the D_0 of each respective gas when diluted with either N_2 or air within the lungs, whereas the selection of b values are reflective of typical in vivo experimental diffusion gradients, which have a maximum gradient strength between 30 to 40 mT/m.[12-23]

All FE simulations were solved using COMSOL Multiphysics (v. 5.3, COMSOL AB, Stockholm, Sweden) on a high-powered computing cluster (Dell PowerEdge C6320) using 12 CPU cores (dual Intel Xeon Processor E5-2630 v3) with 16 GB RAM per core. Boundary conditions assumed impenetrable mesh walls (i.e., 0 flow through the acinar airway walls) on all surfaces, and the initial transverse magnetization was set as 1 to reflect acinar airspaces entirely filled with hyperpolarized gas at the start of each simulation. An entire multiple b value DWI simulation took between 8 to 16 h.

The simulated DWI signal for each b value was averaged across all 31 gradient orientations and every mesh node. The global averaged multiple b value DWI signal was fitted to the CM (with either ^{3}He-based[13] or ^{129}Xe-based[14] expressions) and SEM[15,16] in MATLAB (R2109a, MathWorks) to derive respective diffusion model estimates of acinar airway dimensions for each FE simulation (see Supporting Information for the CM and SEM equations).

2.4 | Validation of in vivo diffusion times

The first set of validation simulations were of hyperpolarized gas DWI in the healthy and IPF acinar airspace meshes with diffusion times of ^{3}He ($\Delta = 1.6$ ms) and ^{129}Xe ($\Delta = 8.5$ ms). For in vivo hyperpolarized gas DWI with the two gases, these respective diffusion times provide comparable diffusion model acinar airway dimensions with both the SEM and CM.[16] ^{3}He diffusion gradient parameters were: $G_{Max} = 31.4$ mT/m, $\Delta = 1.6$ ms, $\delta = 1.6$ ms, and $\tau = 0.3$ ms; ^{129}Xe: $G_{Max} = 32.6$ mT/m, $\Delta = 8.5$ ms, $\delta = 2.9$ ms, and $\tau = 0.3$ ms.

The ^{129}Xe ($\Delta = 8.5$ ms) simulations were fitted to the ^{3}He CM expressions due to in vivo results demonstrating that comparable ^{3}He and ^{129}Xe CM *Lm* can be derived at this diffusion time using the ^{3}He-based expressions.[16]

2.5 | Operational range of theoretical diffusion models

Nine additional ^{129}Xe diffusion times ranging between $\Delta = 5$ and 20 ms were simulated for both healthy and IPF acinar airspace meshes to investigate the relationship between the derived diffusion model parameters and diffusion time and to establish operational ranges for both theoretical diffusion models. ^{129}Xe diffusion gradient parameters for each diffusion time simulation are summarized in Table 1. The respective bipolar gradients for each ^{129}Xe diffusion time were optimized such that similar diffusion gradient amplitudes (G) were implemented at each b value. This ensured that each simulation had a consistent gradient dephasing length $\left(L_G = \sqrt[3]{D_0/\gamma G}\right)$, and that the resulting diffusion regimes were only dependent upon the respective diffusion time or 1D free diffusion length $\left(L_{1D} = \sqrt{2\Delta D_0}\right)$. All diffusion time simulations were fitted to the SEM and ^{129}Xe-based CM expressions, and derived diffusion model parameters were benchmarked against the respective MLI of each acinar airspace mesh.

3 | RESULTS

3.1 | Validation of in vivo diffusion times

A video demonstrating the evolution of the normalized transverse magnetization during a ^{129}Xe ($\Delta = 8.5$ ms) diffusion simulation for each b value in the healthy acinar airspace mesh can be found in Supporting Information Video S1. Table 2 summarizes the global mean SEM- and CM-derived metrics for the ^{3}He and ^{129}Xe FE simulations in the healthy and IPF acinar airspace meshes. For the SEM, the IPF mesh derived a larger global Lm_D and distributions of diffusivity (*DDC*), as well as a smaller alpha heterogeneity index (α) than the healthy mesh for both gases. Across both meshes, the ^{129}Xe α value was larger than the respective ^{3}He α value. For the CM-derived metrics, h was smaller and *Lm* was larger for the IPF mesh, whereas both R and mean alveolar diameter (L_{Alv}) were similar between the healthy and IPF meshes. SEM Lm_D for the healthy mesh demonstrated excellent agreement with the healthy MLI value; however, the Lm_D value for the IPF mesh was 55 and 76 μm smaller than the IPF MLI for ^{3}He and ^{129}Xe simulations, respectively. L_{Alv} and *Lm* derived from the CM were considerably smaller than the respective MLI in both acinar airspace meshes for both gases.

The distributions of Lm_D values across the healthy and IPF acinar airspace meshes for the respective ^{3}He and ^{129}Xe DWI simulations are illustrated in Figure 3; similar distributions of values were also observed for L_{Alv} and *Lm*. In the healthy mesh, smaller acinar airspace dimensions can be observed at the periphery, whereas larger dimensions are found near the center of the mesh corresponding to larger acinar airways. Conversely, the distributions of acinar dimensions in the IPF acinar airspace mesh are more heterogeneous and elevated when compared to the healthy mesh. In both meshes, similar Lm_D distributions were observed for ^{3}He and ^{129}Xe.

3.2 | Operational range of theoretical diffusion models

Table 3 summarizes the ^{129}Xe SEM and CM results for the healthy and IPF acinar airspace meshes simulated at a range of ^{129}Xe diffusion times. The SEM results for ^{129}Xe $\Delta = 8.5$

TABLE 1 Trapezoidal bipolar diffusion gradient parameters for each ^{129}Xe diffusion time FE simulation

^{129}Xe diffusion time (ms)[a]	G_{Max} (mT/m)	Gradient lobe (δ) (ms)	Gradient separation (ms)	L_{1D} (μm)[b]
$\Delta = 5$	31.9	4.1	0.9	374
$\Delta = 6$	32.1	3.6	2.4	410
$\Delta = 7$	31.9	3.3	3.7	443
$\Delta = 8$	32.5	3.0	5.0	473
$\Delta = 9$	31.6	2.9	6.1	502
$\Delta = 10$	32.2	2.7	7.3	529
$\Delta = 13$	31.8	2.4	10.6	603
$\Delta = 16$	31.4	2.2	13.8	669
$\Delta = 20$	31.2	2.0	18.0	748

FE, finite element; L_{1D}, 1D free diffusion length.

[a]For each diffusion time, the same six ^{129}Xe b values (b = 0, 6, 12, 18, 24, 30 s/cm^2) and ramp time (τ) of 0.3 ms were used.

[b]L_{1D} calculated assuming ^{129}Xe free diffusion coefficient (D_0) of 0.14 cm^2/s.

TABLE 2 SEM and CM diffusion model results for FE simulations at the in vivo diffusion times of ^{3}He Δ = 1.6 ms and ^{129}Xe Δ = 8.5 ms

Diffusion Model Metrics		Healthy Mesh		IPF Mesh	
		^{3}He (Δ = 1.6 ms)	^{129}Xe (Δ = 8.5 ms)	^{3}He (Δ = 1.6 ms)	^{129}Xe (Δ = 8.5 ms)
SEM	Lm_D (μm)	258	261	316	295
	DDC (cm^2/s)	0.125	0.0259	0.177	0.0308
	Alpha (α)	0.848	0.924	0.803	0.853
CM	R (μm)	266	290	279	265
	h (μm)	127	142	82	75
	L_{Alv} (μm)	203	222	214	203
	Lm (μm)	168	180	233	225
MLI (μm)		266		371	

Alpha = heterogeneity index; CM, cylinder airway model; DDC = distributed diffusivity coefficient; h = alveolar sleeve depth; IPF = idiopathic pulmonary fibrosis; L_{Alv} = mean alveolar diameter; Lm = mean chord length; Lm_D = mean diffusive length scale; MLI = mean linear intercept length; R = outer acinar airway radius; SEM, stretched exponential model.

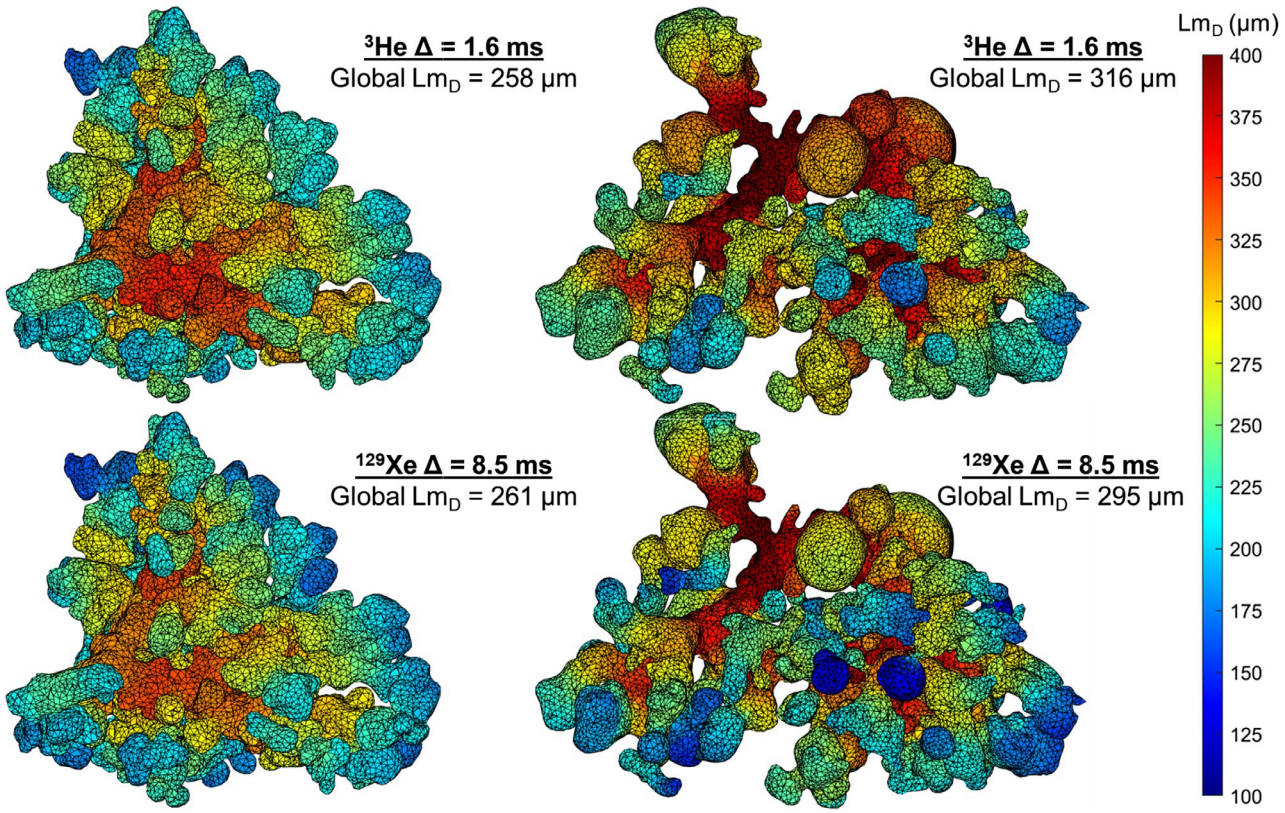

FIGURE 3 Distributions of SEM-derived ^{3}He and ^{129}Xe Lm_D for the healthy and IPF acinar airspace meshes from FE simulations at the typical in vivo imaging diffusion times of ^{3}He Δ = 1.6 ms and ^{129}Xe Δ = 8.5 ms. Lm_D, mean diffusive length scale; SEM, stretched exponential model

ms simulation (Table 2) were included, whereas the CM ^{129}Xe Δ = 8.5 ms results (originally analyzed with ^{3}He CM expressions) were re-analyzed with the ^{129}Xe-based CM expressions. Statistically significant correlations were observed between ^{129}Xe diffusion time and ^{129}Xe Lm_D, DDC, and Lm for both acinar airspace meshes (Table 4). Significant correlations were also observed for R and L_{Alv} in the healthy airspace model only. A logarithmic regression provided the best fit for the DDC and Lm_D data from both acinar airspaces, suggesting a nonlinear relationship between SEM metrics and ^{129}Xe diffusion times (Figure 4A). For the CM Lm metric, a linear relationship with ^{129}Xe diffusion time was observed (Figure 4B).

The best agreement between Lm_D and MLI in the healthy acinar airspace mesh was observed at diffusion times between 8 to 10 ms. In contrast, for the IPF mesh the best agreement between Lm_D and MLI was demonstrated at a 16 ms ^{129}Xe diffusion time. A large mismatch between Lm and MLI was

TABLE 3 SEM and CM diffusion model results for FE simulations across a range of ^{129}Xe diffusion times

		Healthy Mesh							IPF Mesh					
^{129}Xe Δ (ms)	L_{1D} (μm)	Lm_D (μm)	*DDC* (cm^2/s)	Alpha (α)	*R* (μm)	*h* (μm)	L_{Alv} (μm)	*Lm* (μm)	Lm_D (μm)	*DDC* (cm^2/s)	Alpha (α)	*R* (μm)	*h* (μm)	L_{Alv} (μm)	*Lm* (μm)
Δ = 5	374	218	0.0303	0.912	356	214	273	197	240	0.0337	0.825	444	253	340	253
Δ = 6	410	230	0.0291	0.929	274	126	210	177	258	0.0356	0.907	278	93	213	216
Δ = 7	443	246	0.0271	0.904	269	115	206	182	280	0.0348	0.893	283	84	216	234
Δ = 8	473	256	0.0262	0.907	287	128	220	189	295	0.0326	0.852	281	76	215	245
Δ = 8.5	488	261	0.0259	0.924	313	156	240	193	295	0.0308	0.853	279	79	213	237
Δ = 9	502	263	0.0253	0.933	320	164	245	195	298	0.0304	0.877	312	112	238	232
Δ = 10	529	270	0.0248	0.940	346	188	265	203	316	0.0302	0.858	304	91	232	250
Δ = 13	603	289	0.0226	0.951	410	256	313	221	334	0.0260	0.864	332	122	254	244
Δ = 16	669	314	0.0208	0.943	411	245	315	228	376	0.0265	0.848	356	117	272	278
Δ = 20	748	335	0.0186	0.929	422	249	323	235	400	0.0247	0.879	420	175	322	287
MLI		266							371						

observed across this range of ^{129}Xe diffusion times, with the closest agreement of 11.7% and 22.6% difference obtained at a ^{129}Xe diffusion time of 20 ms for the healthy and IPF meshes, respectively.

4 | DISCUSSION

In this work, we have developed realistic acinar airspace geometrical meshes from 3D micro-CT imaging and utilized them for FE simulations of hyperpolarized ^{3}He and ^{129}Xe DWI to validate the SEM and its Lm_D measurement alongside the CM.

4.1 | Validation of in vivo diffusion times

FE simulations of ^{3}He and ^{129}Xe multiple *b* value DWI at the commonly reported in vivo diffusion times of ^{3}He Δ = 1.6 ms[13,15,22,38] and ^{129}Xe Δ = 8.5 ms[16,29] were performed. The global diffusion metrics, derived from both the SEM and CM, from the healthy acinar airway mesh were in agreement with those acquired from healthy volunteers with the same ^{3}He and ^{129}Xe DWI acquisition parameters.[29] The simulated Lm_D from the healthy acinar mesh was larger than those found in previous in vivo studies of healthy volunteers even with the same *DDC* and α because the integrals in Equations [S5] and [S8] now have an upper limit of infinity instead of D_0 and L_{1D}, respectively. The ^{3}He and ^{129}Xe diffusion metrics for the IPF mesh were smaller than those reported for in vivo patients with IPF.[22,29] However, these reported IPF lung values are global averages and are likely to be different to those derived from a single acinar airspace region selected from a single ex vivo IPF lung sample. The smaller α values found for the IPF mesh, when compared to the healthy mesh, are characteristic of the increased heterogeneity of IPF acinar airspaces. The increased heterogeneity and elevated IPF Lm_D values match the results observed in IPF patients with in vivo ^{3}He DWI[22] and are indicative of the microstructural acinar changes related to fibrotic disease.

The global ^{3}He and ^{129}Xe Lm_D value in the healthy mesh at the in vivo diffusion times were in excellent agreement with the MLI of the healthy acinar mesh. The underestimation of IPF Lm_D values with MLI is comparable to the bias observed previously with histological validation of ^{3}He *Lm*.[13] The larger mismatch observed between Lm_D and MLI in the IPF geometry in comparison to the healthy geometry could be attributed to the larger percentage of IPF intercept lengths (Figure 2B), which are greater than the respective L_{1D} derived from the ^{3}He (L_{1D} = 530 μm) and ^{129}Xe (L_{1D} = 488 μm) FE simulations, respectively. In a given diffusion experiment, gas atoms will experience D_0 in length scales far greater than L_{1D}. Therefore, in acinar airspace dimensions that are far

TABLE 4 Correlations between ^{129}Xe diffusion time and SEM and CM diffusion model metrics

	SEM			CM			
r (P)[a]	Lm_D (μm)	DDC (cm^2/s)	Alpha (α)	R (μm)	h (μm)	L_{Alv} (μm)	Lm (μm)
Healthy	0.987 (< 0.001)**	−0.980 (< 0.001)**	0.543 (0.105)	0.816 (0.004)**	0.105 (0.773)	0.816 (0.004)*	0.925 (< 0.001)**
IPF	0.985 (< 0.001)**	−0.926 (< 0.001)**	0.013 (0.971)	0.404 (0.247)	0.137 (0.706)	0.404 (0.247)	0.820 (0.004)*

[a]Pearson correlation coefficient.

*Significance at the $P < .01$ level.

**Significance at the $P < .001$ level.

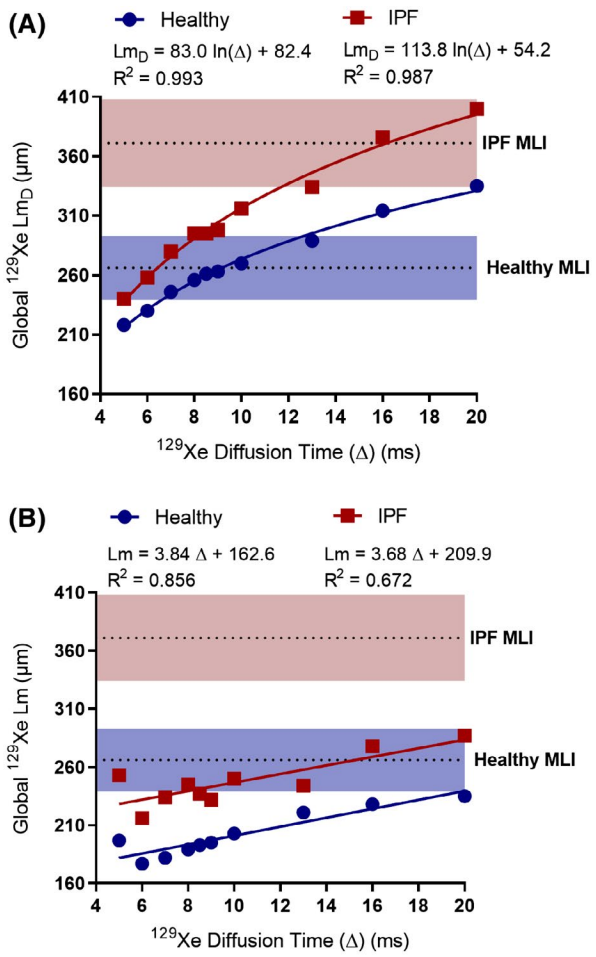

FIGURE 4 Plots of global ^{129}Xe SEM Lm_D (A) and CM Lm (B) derived from FE simulations across a range of ^{129}Xe diffusion times for both healthy and IPF acinar airspace meshes. A nonlinear logarithmic and linear relationship was observed between ^{129}Xe diffusion time and Lm_D and Lm, respectively. The dotted lines represent the MLI of the healthy and IPF acinar airspace mesh. The shaded boxes encompass ±10% of the respective MLI value and represent the confidence interval for agreement of Lm_D and Lm with MLI. CM, cylinder airway model; Lm, mean chord length; MLI, mean linear intercept length

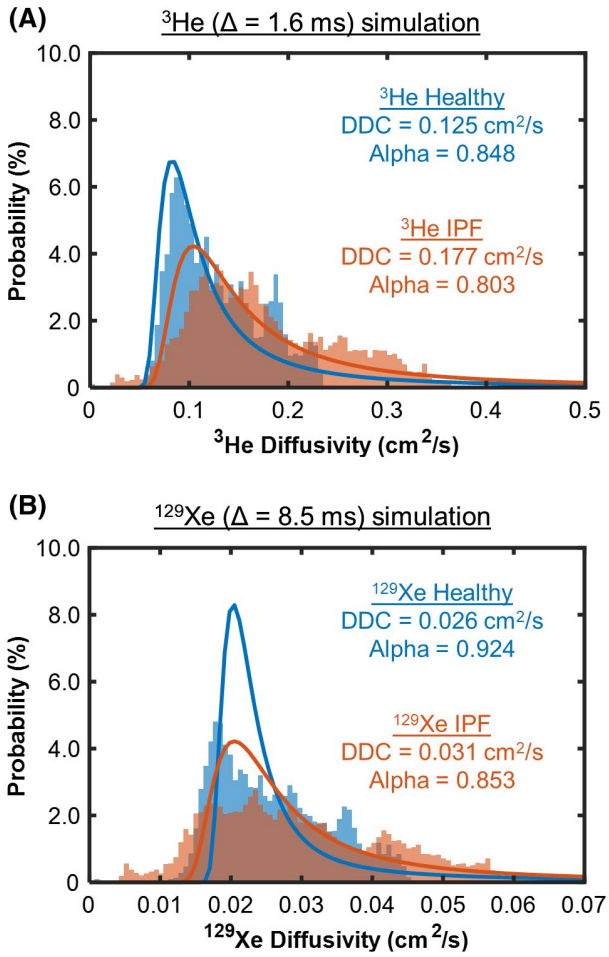

FIGURE 5 SEM $p(D)$ for each acinar airspace model for the (A) ^{3}He (Δ = 1.6 ms) and (B) ^{129}Xe (Δ = 8.5 ms) FE simulations derived from the global DDC and alpha values. Each $p(D)$ is plotted against DDC values evaluated at each mesh node and represents the true underlying distribution of apparent diffusivities of each respective simulation. The similar shapes of $p(D)$ and DDC distributions demonstrate that the SEM $p(D)$ is representative of intravoxel distribution of diffusivities. DDC, distributed diffusivity coefficient; $p(D)$, probability distribution of diffusivities

greater than L_{1D}, a Lm_D value equivalent to L_{1D} will be derived by the SEM.

To investigate whether the probability distribution of diffusivities $p(D)$ derived from the SEM are an accurate representation of the underlying intravoxel distribution of apparent diffusivities, $p(D)$ were generated from global DDC and α values (Table 2) for the ^{3}He (Δ = 1.6 ms) and ^{129}Xe (Δ = 8.5 ms) FE simulations in the healthy and IPF airway meshes (Figure 5). The shape of the $p(D)$ was compared to histogram distributions of DDC values evaluated

at each mesh node for each respective FE simulation. The similar shapes of the $p(D)$ and the *DDC* distribution confirms that the SEM $p(D)$ does indeed reflect the underlying intravoxel diffusivities. It is important to note that the distributions in Figure 5 are representative of intravoxel distributions of diffusivity (*DDC*), and as such they are different to histograms of *ADC* or *DDC* values averaged across numerous voxels from images of the whole lungs typically reported in the literature.

In contrast to the SEM, the CM acinar dimension metrics of L_{Alv} and *Lm* were both much smaller than the healthy and IPF meshes' MLI. The mismatch of ~100 μm between simulated ^{3}He and ^{129}Xe *Lm* and MLI is greater than the average ~20 μm bias observed between ^{3}He *Lm* and MLI in histological validation of the CM.[13] This difference could perhaps be associated with sample bias of histological tissue samples when compared to whole lung ^{3}He DWI measurements or from lung inflation differences due to shrinkage of lung tissue between ^{3}He DWI measurements and the subsequent fixation process for histological measurements. These potential inaccuracies are absent in these FE simulations due to the calculation of MLI across the entire acinar airspace model that is compared to simulated hyperpolarised gas DWI in the same geometry.

The small difference between ^{3}He and ^{129}Xe Lm_D in the healthy mesh further supports the implementation of ^{129}Xe $\Delta = 8.5$ ms for in vivo ^{129}Xe DWI.[16] The larger discrepancy between healthy and IPF meshes could be explained by two factors. First, the ^{129}Xe $\Delta = 8.5$ ms was optimized by measurements from a single healthy subject[16]; as such, in patients with more heterogeneous distributions of acinar length scales, perhaps a different optimal diffusion time exists. The results in Table 3 suggest that for the IPF mesh the optimal ^{129}Xe diffusion time is 10 ms. Second, additional effects on diffusion signal from microscopic background susceptibility gradients[39] are not accounted for in these FE simulations.

4.2 | Operational range of theoretical diffusion models

The second set of validation experiments for the SEM and CM were simulations of ^{129}Xe diffusion times between 5 and 20 ms within the healthy and IPF meshes. This range encompasses the optimal ^{129}Xe $\Delta = 5$ ms for the ^{129}Xe CM expressions[14] and ^{129}Xe $\Delta = 20$ ms that has a L_{1D} corresponding to approximately the mean length of a healthy acinar duct (730 μm).[40] This mean acinar duct length is of particular significance to the CM geometrical model, where if an in vivo experiment's L_{1D} exceeds this length, the underlying assumption that the majority of hyperpolarized gas atoms are contained within the same acinar unit in the diffusion time is no longer correct, and the assumption of anisotropic diffusion is thus no longer valid.

Significant correlations of ^{129}Xe diffusion metrics from both the SEM and CM with ^{129}Xe diffusion time were observed, demonstrating the dependency of diffusion model–derived metrics on experimental diffusion time. The diffusion time dependency reflects the L_{1D} of the experiment, assuming a constant D_0. L_{1D} or diffusion time is a dependent variable in both the SEM[15,16] and CM[13,14] diffusion model expressions. Therefore, it is not surprising that the majority of diffusion model metrics demonstrated a correlation with experiment diffusion time or L_{1D}.

The alpha heterogeneity index (α) from the SEM was the only diffusion model metric not significantly correlated with diffusion time. α represents the deviation of the diffusion signal decay from a mono-exponential decay due to different acinar structures of varying sizes and orientations that lead to different apparent diffusion rates and has been demonstrated to be independent of experimental conditions such as lung inflation.[41] Therefore, in these ^{129}Xe diffusion time simulations where the underlying acinar airspace structure is constant, the α value for each respective acinar airspace mesh is relatively similar across all diffusion times. The small differences in α for the range of ^{129}Xe diffusion times likely reflect small changes to diffusion signal behavior related to differences in L_{1D}.

Nonlinear logarithmic relationships were observed between some of the ^{129}Xe SEM metrics and ^{129}Xe diffusion time. The logarithmic decay of *DDC* is similar to that observed with ^{3}He and ^{129}Xe ADC in healthy volunteers.[16,42] For SEM Lm_D, the positive logarithmic relationship suggests that with increasing diffusion time there is an asymptotic plateauing of Lm_D. A linear correlation between ^{129}Xe diffusion time and Lm_D was observed previously in vivo in one healthy volunteer.[16] This difference could be attributed to the inclusion of more diffusion times in these FE simulations, especially those greater than ^{129}Xe $\Delta = 10$ ms that have not yet been explored experimentally in vivo either due to SNR or breath-hold limitations.

A linear regression fit best described the significant correlation between CM *Lm* and ^{129}Xe diffusion time. Across both acinar airspace models, a small increase in *Lm* can be observed with increasing diffusion time (Figure 4B), which could be related to the relative independence of some underlying phenomenological expressions of the CM to diffusion time.[14] Larger differences between the CM *Lm* and MLI, when compared to SEM Lm_D across this range of diffusion times, are likely related to the small optimal diffusion time range of $\Delta = 4$ to 6 ms for the ^{129}Xe-based CM expressions.[14] Furthermore, the large differences between CM *Lm* and MLI in the IPF mesh could also be associated with the underlying CM geometrical model, which assumes the interstitial space between alveolus units is < 10μm and negligible in the derivation of *Lm*.[13] Therefore, the CM expressions are not necessarily valid for the thickened (fibrosed) interstitium in IPF disease and may be more relevant in chronic obstructive pulmonary disease lungs .

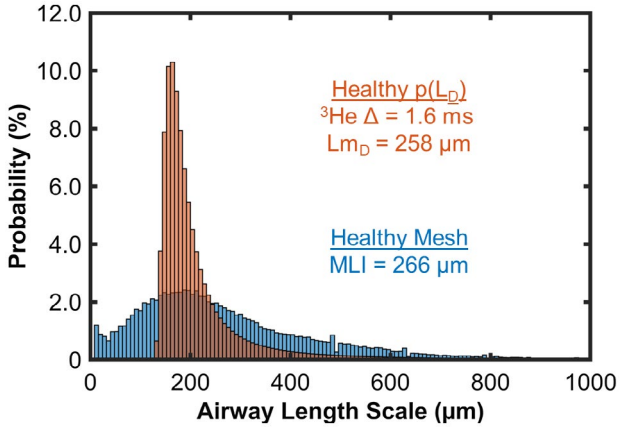

FIGURE 6 Comparison of the healthy acinar airspace mesh linear intercept length distribution (blue) and $p(L_D)$ for the ^{3}He $\Delta = 1.6$ ms simulation (red). The $p(L_D)$ is derived from the $p(D)$ with the following expression: $\int_0^\infty p\left(L_D\right) dL_D = \int_0^\infty p\left(D\right) dD/dL_D dL_D$. Although the global Lm_D from the $p(L_D)$ matches the MLI, the shapes of the two distributions of airway length scale are different. (Note: both histograms are normalized and have the same 8 μm bin width). $p(L_D)$, probability distribution of diffusive length scale

The best agreement between Lm_D and MLI in the healthy and IPF acinar airspace meshes was observed at diffusion times of 9 ms and 16 ms, respectively. This difference can be attributed to the differences in underlying length scales of each acinar airspace model. If we define a confidence interval of Lm_D values within ±10% of the MLI (Figure 4A), the operational ranges of diffusion time for the healthy and IFP meshes are defined as between 7 to 13 ms, and 13 to 20 ms, respectively. Although this may suggest that in vivo acquisitions at longer diffusion times may provide better direct correspondence with MLI, additional effects related to longer diffusion times such as increased T_2* decay and longer acquisition times, which in turn meaning longer breath-holds, prevent this from being applied routinely for in vivo imaging. The currently implemented in vivo ^{129}Xe $\Delta =$ 8.5 ms allows for the 3D whole lung acquisitions in a single breath-hold.[16] Furthermore, at this diffusion time we observe excellent agreement with MLI in healthy acinar length scales, and in larger length scales systematic differences between healthy and diseased acinar airspaces are still detected.

The differences in diffusion time operational ranges for the healthy and IPF lung simulations can be attributed to inherent differences between the apparent length scale (Lm_D) from diffusion models and MLI from histology. This is illustrated in Figure 6 for the probability distribution of diffusive length scales, $p\left(L_D\right)$, and MLI histogram of the healthy airspace mesh. Figure 6 represents intravoxel distributions of length scale derived theoretically with the SEM $p\left(L_D\right)$ (red) or from histological intercept lengths (blue). The differences in the histogram tails are related to the L_{1D} constraints of the diffusion experiment where there is a plateauing of L_D toward L_{1D}. The absence of small L_D (<150 μm) in the $p\left(L_D\right)$ can be attributed to diffusion motional averaging effects in these small airway dimensions (see Figure 3 of Yablonskiy et al[12]). The combination of these two effects could account for the different diffusion time operational ranges for the two sets of airways. Further FE simulations in a wider range of different airway length scales could be performed in order to derive a mathematical transformation that will allow a derived $p\left(L_D\right)$ to be mapped to the underlying airway distribution across a variety of diffusion experimental parameters. This is akin to the approach used to establish CM phenomenological expressions (eg, Equations 3 and 4 in Ref. 43) that describe the relationship between anisotropic diffusion coefficients and cylindrical airway geometry parameters.[14,43]

4.3 | FE simulations limitations and assumptions

The micro-CT–derived acinar airspace meshes are, to our knowledge, the most realistic airway geometry used to date for the simulation and validation of hyperpolarized gas DWI signal behavior within the lungs. Although these acinar airspace meshes represent single connected acinar airspace geometries approximately the size of a MR voxel, they may not be representative of the acinar airway variation across the whole lung. However, it should be noted that the linear intercept length distribution of the healthy FE model is representative of the larger (14 mm diameter) micro-CT lung core sample from which the healthy FE model was derived (see Supporting Information Figure S1). Future FE simulations could be performed in larger acinar airspace meshes that represent acinar geometry on a lobar or segmental level.

One limitation of the micro-CT MLI is the inherent resolution (16 μm) of the micro-CT imaging. To improve the accuracy of linear intercept length measurements, segmented acinar airspace masks were up-sampled to an isotropic 4 μm resolution. Even with up-sampling, intercept lengths are only accurate to the nearest 4 μm increment, which is substantially larger than the typical submicron resolution of histological section images obtained with light microscopy for MLI calculation.[32] However, the process of sampling intercept length measurements across the entire acinar airspace geometry in this work allows for the direct comparison of histology and diffusion measurements in identical regions of acinar airspace. Furthermore, this eliminates any potential sampling bias that may occur from conventional histological assessment of lung tissue samples used in previous validation studies.[13]

The absence of simulated SEM and CM metrics in lung meshes representing emphysema lung disease is a limitation of this work. Future FE simulations in a micro-CT–derived emphysema lung model would be beneficial and would complement the diffusion model validations shown here in healthy and IPF lungs. In addition, the CM diffusion model

may be more accurate in an emphysema lung mesh due to the optimization of the CM for evaluating emphysematous alveolar changes.[12,13]

Our FE simulations of hyperpolarized gas DWI assume that the change in transverse magnetization is entirely due to diffusion of ^{3}He or ^{129}Xe gas atoms during the duration of bipolar trapezoidal waveforms. Therefore, additional effects on in vivo hyperpolarized gas DWI signal behavior such as background susceptibility gradients, RF depletion, T_1 decay, and signal change due to dissolved ^{129}Xe in the interstitium are not currently accounted for. Typically, with the small flip angles and short TR used for in vivo imaging, the majority of these effects have negligible influence on the hyperpolarized gas DWI signal behavior and diffusion model metrics. However, the presence of background susceptibility gradients due to the susceptibility differences between the lung parenchyma and oxygenated airspaces have been shown to influence in vivo ADC and diffusion model measurements[39] and are also field strength–dependent.[38] The absence of a tissue–air susceptibility interface in the FE models means that the simulation results are not a complete mechanistic representation of the signal formation of in vivo hyperpolarized gas DWI. Future FE simulations that incorporate a susceptibility difference at the boundaries of the FE model with a B_0 term could be used to further investigate the effects of background susceptibility gradients on diffusion model–derived metrics.

5 | CONCLUSION

This work is the first validation of the SEM-derived Lm_D and the CM Lm with FE simulations of ^{3}He and ^{129}Xe DWI in micro-CT–derived realistic acinar airway geometries representing healthy and IPF lungs. The SEM Lm_D demonstrated better agreement with MLI when compared to the CM Lm across each FE simulation and acinar mesh. Excellent agreement ($\pm$10% difference) between Lm_D and MLI was observed in FE simulations at ^{3}He ($\Delta = 1.6$ ms) and ^{129}Xe ($\Delta = 7$ to 13 ms), and ^{129}Xe ($\Delta = 13$ to 20 ms) for the healthy and IPF acinar meshes, respectively. This further validates previous experimental demonstrations of the use of the SEM for accurate estimation of lung microstructural dimensions and indicates that the SEM is relatively robust across a range of experimental conditions and acinar length scales.

ACKNOWLEDGMENT

The authors would like to thank Dr. Bart Vanaudenaerde and Dr. John McDonough of Catholic University Leuven and Dr. James Hogg of University of British Columbia for sharing micro-CT images of ex vivo lung tissue samples. This work was supported by National Institute for Health Research (NIHR) grant NIHR-RP-R3-12-027 and Medical Research Council (MRC) grant MR/M008894/1. The views expressed in this publication are those of the authors and not necessarily those of the National Health Service, the National Institute for Health Research, or the Department of Health.

ORCID

Ho-Fung Chan https://orcid.org/0000-0002-5382-2097
Guilhem J. Collier https://orcid.org/0000-0002-1874-4775

REFERENCES

1. Gould GA, MacNee W, McLean A, et al. CT measurements of lung density in life can quantitate distal airspace enlargement—an essential defining feature of human emphysema. *Am Rev Respir Dis*. 1988;137:380-392.
2. Gevenois PA, Yernault JC. Can computed tomography quantify pulmonary emphysema? *Eur Respir J*. 1995;8:843-848.
3. Uppaluri R, Mitsa T, Sonka M, et al. Quantification of pulmonary emphysema from lung computed tomography images. *Am J Respir Crit Care Med*. 1997;156:248-254.
4. Bartholmai BJ, Raghunath S, Karwoski RA, et al. Quantitative computed tomography imaging of interstitial lung diseases. *J Thorac Imaging*. 2013;28:298-307.
5. Maldonado F, Moua T, Rajagopalan S, et al. Automated quantification of radiological patterns predicts survival in idiopathic pulmonary fibrosis. *Eur Respir J*. 2014;43:204-212.
6. King GG, Muller NL, Pare PD. Evaluation of airways in obstructive pulmonary disease using high-resolution computed tomography. *Am J Respir Crit Care Med*. 1999;159:992-1004.
7. Weibel ER. *Morphometry of the Human Lung*. Berlin-Heidelberg, Germany: Springer; 1963.
8. McDonough JE, Yuan R, Suzuki M, et al. Small-airway obstruction and emphysema in chronic obstructive pulmonary disease. *N Engl J Med*. 2011;365:1567-1575.
9. Hogg JC, McDonough JE, Suzuki M. Small airway obstruction in COPD. *Chest*. 2013;143:1436-1443.
10. Saam BT, Yablonskiy DA, Kodibagkar VD, et al. MR imaging of diffusion of 3He gas in healthy and diseased lungs. *Magn Reson Med*. 2000;44:174-179.
11. Kaushik SS, Cleveland ZI, Cofer GP, et al. Diffusion-weighted hyperpolarized 129Xe MRI in healthy volunteers and subjects with chronic obstructive pulmonary disease. *Magn Reson Med*. 2011;65:1154-1165.
12. Yablonskiy DA, Sukstanskii AL, Leawoods JC, et al. Quantitative in vivo assessment of lung microstructure at the alveolar level with hyperpolarized 3He diffusion MRI. *Proc Natl Acad Sci U S A*. 2002;99:3111-3116.
13. Yablonskiy DA, Sukstanskii AL, Woods JC, et al. Quantification of lung microstructure with hyperpolarized 3He diffusion MRI. *J Appl Physiol (1985)*. 2009;107:1258-1265.
14. Sukstanskii AL, Yablonskiy DA. Lung morphometry with hyperpolarized 129Xe: theoretical background. *Magn Reson Med*. 2012;67:856-866.
15. Chan HF, Stewart NJ, Parra-Robles J, Collier GJ, Wild JM. Whole lung morphometry with 3D multiple b-value hyperpolarized gas MRI and compressed sensing. *Magn Reson Med*. 2017;77:1916-1925.
16. Chan HF, Stewart NJ, Norquay G, Collier GJ, Wild JM. 3D diffusion-weighted (129) Xe MRI for whole lung morphometry. *Magn Reson Med*. 2018;79:2986-2995.

17. Quirk JD, Lutey BA, Gierada DS, et al. In vivo detection of acinar microstructural changes in early emphysema with (3)He lung morphometry. *Radiology*. 2011;260:866-874.
18. Hajari AJ, Yablonskiy DA, Sukstanskii AL, Quirk JD, Conradi MS, Woods JC. Morphometric changes in the human pulmonary acinus during inflation. *J Appl Physiol (1985)*. 2012;112:937-943.
19. Butler JP, Loring SH, Patz S, Tsuda A, Yablonskiy DA, Mentzer SJ. Evidence for adult lung growth in humans. *N Engl J Med*. 2012;367:244-247.
20. Fishman EF, Quirk JD, Sweet SC, et al. What makes a good pediatric transplant lung: insights from in vivo lung morphometry with hyperpolarized 3 He magnetic resonance imaging. *Pediatr Transplant*. 2017;21:e12886
21. Quirk JD, Sukstanskii AL, Woods JC, et al. Experimental evidence of age-related adaptive changes in human acinar airways. *J Appl Physiol (1985)*. 2016;120:159-165.
22. Chan HF, Weatherley ND, Johns CS, et al. Airway microstructure in idiopathic pulmonary fibrosis: assessment at hyperpolarized (3) He diffusion-weighted MRI. *Radiology*. 2019;291:223-229.
23. Quirk JD, Chang YV, Yablonskiy DA. In vivo lung morphometry with hyperpolarized (3)He diffusion MRI: reproducibility and the role of diffusion-sensitizing gradient direction. *Magn Reson Med*. 2015;73:1252-1257.
24. Hajari AJ, Yablonskiy DA, Quirk JD, et al. Imaging alveolar-duct geometry during expiration via (3)He lung morphometry. *J Appl Physiol (1985)*. 2011;110:1448-1454.
25. Wang W, Nguyen NM, Yablonskiy DA, et al. Imaging lung microstructure in mice with hyperpolarized 3He diffusion MRI. *Magn Reson Med*. 2011;65:620-626.
26. Parra-Robles J, Ajraoui S, Deppe MH, et al. Experimental investigation and numerical simulation of 3He gas diffusion in simple geometries: implications for analytical models of 3He MR lung morphometry. *J Magn Reson*. 2010;204:228-238.
27. Sukstanskii AL, Conradi MS, Yablonskiy DA. (3)He lung morphometry technique: accuracy analysis and pulse sequence optimization. *J Magn Reson*. 2010;207:234-241.
28. Parra-Robles J, Wild JM. The influence of lung airways branching structure and diffusion time on measurements and models of short-range 3He gas MR diffusion. *J Magn Reson*. 2012;225:102-113.
29. Chan HF,Collier GJ, Weatherley ND, Wild JM. Comparison of in vivo lung morphometry models from 3D multiple b-value (3) He and (129) Xe diffusion-weighted MRI. *Magn Reson Med*. 2019;81:2959-2971.
30. Mai C, Verleden SE, McDonough JE, et al. Thin-section CT features of idiopathic pulmonary fibrosis correlated with micro-CT and histologic analysis. *Radiology*. 2017;283:252-263.
31. Parra-Robles J, Vasilescu D, Hogg JC, Wild JM. Modelling of 3He gas diffusion in realistic 3D models of human acinar airways obtained from micro-CT images. *Eur Respir J*. 2014;44(suppl 58):P4972.
32. Hsia CC, Hyde DM, Ochs M, Weibel ER. An official research policy statement of the American Thoracic Society/European Respiratory Society: standards for quantitative assessment of lung structure. *Am J Respir Crit Care Med*. 2010;181:394-418.
33. Knudsen L, Weibel ER, Gundersen HJ, Weinstein FV, Ochs M. Assessment of air space size characteristics by intercept (chord) measurement: an accurate and efficient stereological approach. *J Appl Physiol (1985)*. 2010;108:412-421.
34. Thomen RP, Quirk JD, Roach D, et al. Direct comparison of (129) Xe diffusion measurements with quantitative histology in human lungs. *Magn Reson Med*. 2017;77:265-272.
35. Woods JC, Choong CK, Yablonskiy DA, et al. Hyperpolarized 3He diffusion MRI and histology in pulmonary emphysema. *Magn Reson Med*. 2006;56:1293-1300.
36. Stejskal EO, Tanner JE. Spin diffusion measurements: spin echoes in the presence of a time-dependent field gradient. *J Chem Phys*. 1965;42:288.
37. Torrey HC. Bloch equations with diffusion terms. *Phys Rev*. 1956;104:563-565.
38. Parra-Robles J, Ajraoui S, Marshall H, Deppe MH, Xu X, Wild JM. The influence of field strength on the apparent diffusion coefficient of 3He gas in human lungs. *Magn Reson Med*. 2012;67:322-325.
39. Mugler J III, et al. Evidence of background-gradient effects in GRE-based 3He diffusion MRI. In Proceedings of the 14th Annual Meeting of ISMRM, Seattle, WA, 2006. Abstract 1313.
40. Haefeli-Bleuer B, Weibel ER. Morphometry of the human pulmonary acinus. *Anat Rec*. 1988;220:401-414.
41. Parra-Robles J, Marshall H, Wild JM. Characterization of 3He diffusion in lungs using a stretched exponential model. In Proceedings of the 21st Annual Meeting of ISMRM, Salt Lake City, UT, 2013, p. 820.
42. Gierada DS, Woods JC, Bierhals AJ, et al. Effects of diffusion time on short-range hyperpolarized (3)He diffusivity measurements in emphysema. *J Magn Reson Imaging*. 2009;30:801-808.
43. Sukstanskii AL, Yablonskiy DA. In vivo lung morphometry with hyperpolarized 3He diffusion MRI: theoretical background. *J Magn Reson*. 2008;190:200-210.

SUPPORTING INFORMATION

Additional Supporting Information may be found online in the Supporting Information section.

FIGURE S1 (A) Example micro-CT image slice of one healthy lung core sample used to create the healthy acinar airspace FE model (blue mask). (B) For the same example micro-CT image slice, acinar airspace segmentation mask (red) across the whole micro-CT volume. (C) Histogram distributions (16 μm bin widths) for intercept lengths calculated across the healthy FE model volume (blue) and the entire healthy micro-CT lung core sample (red)

TABLE S1 Mesh size optimization results for FE simulations of a ^{3}He diffusion (Δ = 1.6 ms) with a single b-value (b = 1.6 s/cm^2) in the healthy acinar airspace mesh

VIDEO S1 The evolution of the normalized transverse magnetization during a ^{129}Xe (Δ = 8.5 ms) diffusion simulation for each non-zero b-value (b = 6, 12, 18, 24, 30 s/cm^2) in the healthy acinar airspace FE mesh

How to cite this article: Chan H-F, Collier GJ, Parra-Robles J, Wild JM. Finite element simulations of hyperpolarized gas diffusion MRI in micro-CT meshes of acinar airways: validating the cylinder and stretched exponential models of lung microstructural length scales. *Magn Reson Med*. 2021;00:1–12. https://doi.org/10.1002/mrm.28703